Electronic Supplementary Information (ESI) for

Highly sensitive wireless nitrogen dioxide gas sensor based on organic conductive nanocomposite paste

Sung Gun Kim[a], Jaemoon Jun[a, b], Jun Seop Lee[c]*, and Jyongsik Jang[a]*

[a] School of Chemical and Biological Engineering, College of Engineering, Seoul National University, 599 Gwanangno, Gwanakgu, Seoul, 151-742 (Korea),

[b] LG Chem R&D Campus Daejeon, 188, Munji-ro, Yuseong-gu, Daejeon, 34122, Republic of Korea

[c] Department of Materials Science and Engineering, Gachon University, 1342 Seongnamdaero, Sujeong-gu, Seongnam-Si, Gyeonggi-Do, 13120 (Korea)

Corresponding Author:

*E-mail: (J. Jang) jsjang@plaza.snu.ac.kr; Tel.: +82-2-880-7069; Fax: +82-2-880-1604

*E-mail: (J.S. Lee) junseop@gachon.ac.kr; Tel.: +82-31-750-5814; Fax: +82-31-750-5389

1. Schematic diagram of the M_FeHNPs

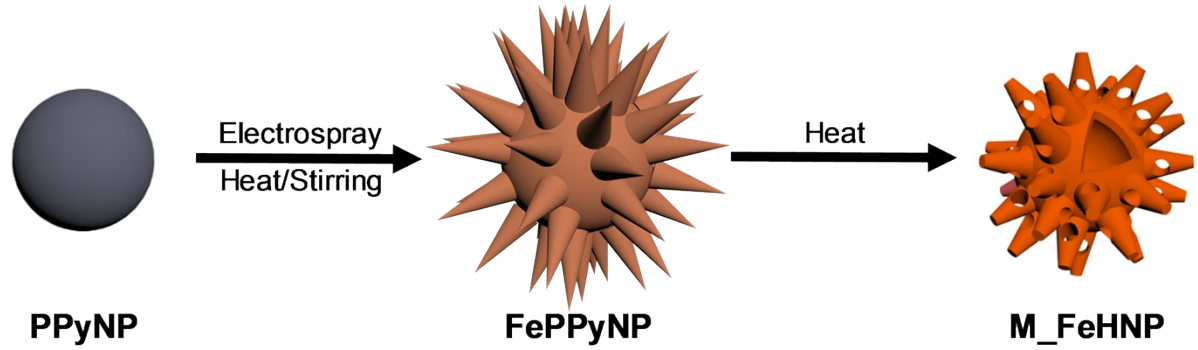

Figure S1. Schematic illustration diagram for a fabrication of the multidimensional Fe_2O_3 hollow nanoparticles (M_FeHNPs).

2. TEM images of each step nanoparticles

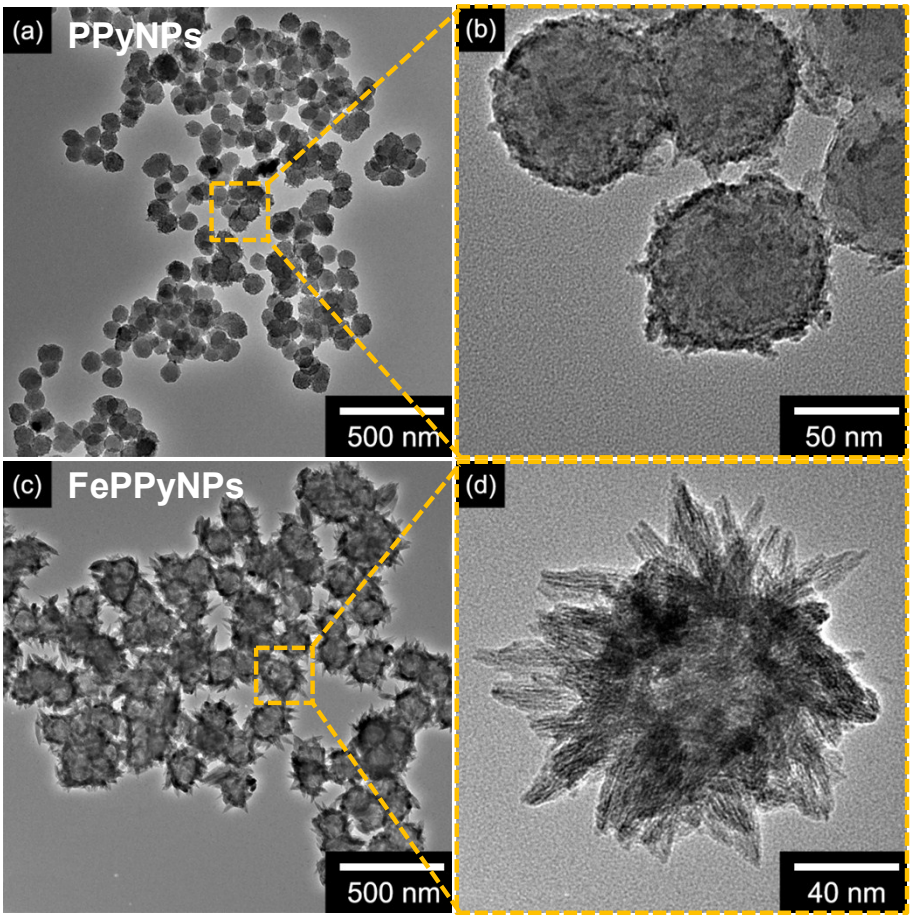

Figure S2. Low and high magnification of TEM images for each synthesis step particles ((a) and (b): polypyrrole nanoparticles (PPyNP); (c) and (d): FeOOH needle decorated polypyrrole nanoparticles (FePPyNP)).

3. XRD patterns of the nanoparticles

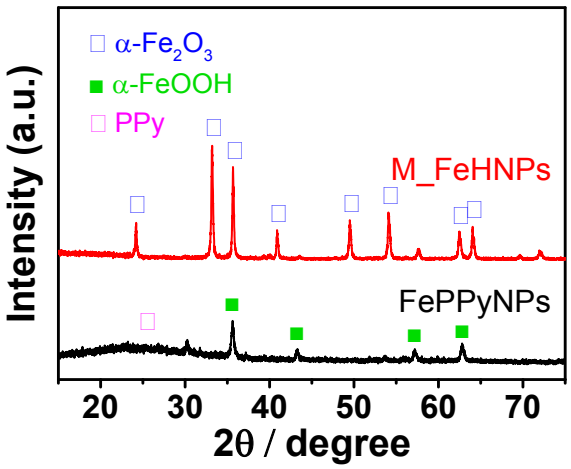

Figure S3. X-ray diffraction (XRD) of FePPyNPs (black) and M_FeHNPs (red).

To characterize of the crystalline structure of each step nanoparticles, X-ray diffraction (XRD) analysis is conducted as shown in **Figure S3**. The narrow peaks of the FeOOH-decorated nanoparticles (FePPyNPs) indicate α-FeOOH (JCPDS 29-713) and the broad peak around 25.6 cm^{-1} of the particle suggests polypyrrole core in the structure. On the other hand, M_FeHNPs present narrow peaks of α-Fe_2O_3 (JCPDS 84-0311) without broad peak because of phase transfer of FeOOH to Fe_2O_3 with pyrolysis of polypyrrole core during calcination step.

4. Schematic diagram of the organic conductive paste

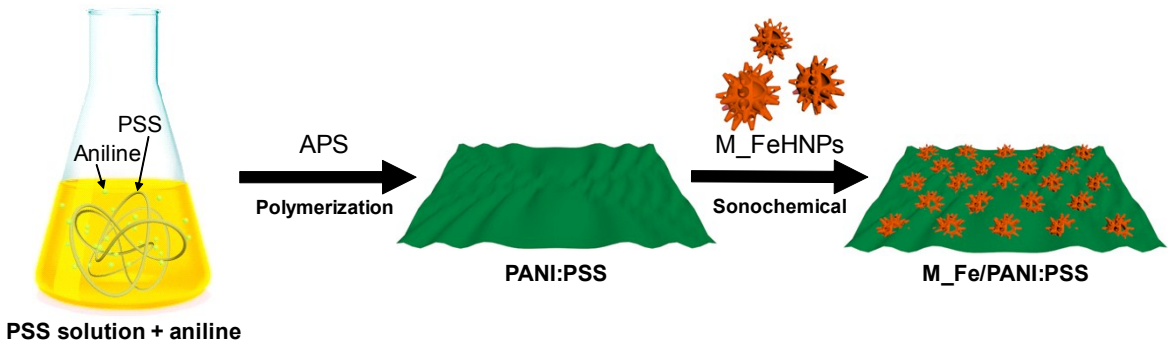

Figure S4. Illustrative diagram of the sequential fabrication for the organic conductive nanocomposite (M_Fe/PANI:PSS) paste.

5. Organic conductive paste-deposited IDA electrode

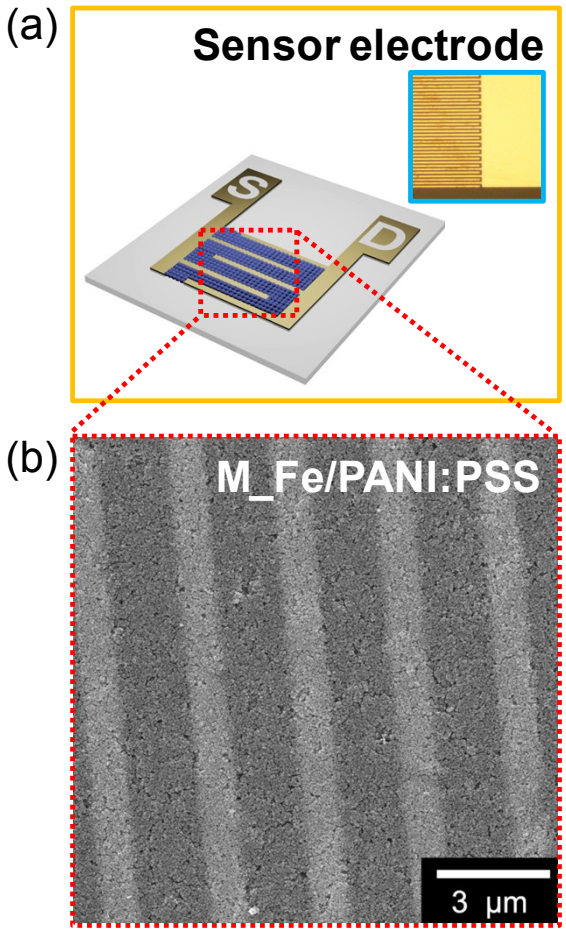

Figure S5. (a) Schematic illustration of the M_Fe/PANI:PSS paste-deposited interdigitated array (IDA) electrode (inset : optical microscopy image of the IDA electrode). (b) FE-SEM image of the M_Fe/PANI:PSS-deposited electrode.

6. Electrical properties of the conductive paste on the IDA electrode

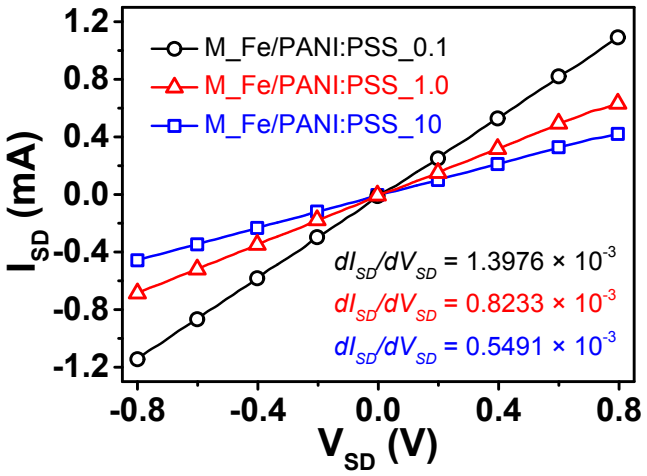

Figure S6. Current-voltage (*I-V*) curves for the different M_Fe/PANI:PSS paste-deposited IDA electrodes (M_Fe/PANI:PSS_0.1: black; M_Fe/PANI:PSS_1: red; M_Fe/PANI:PSS_10: blue).

7. Energy band gap of the nanocomposite

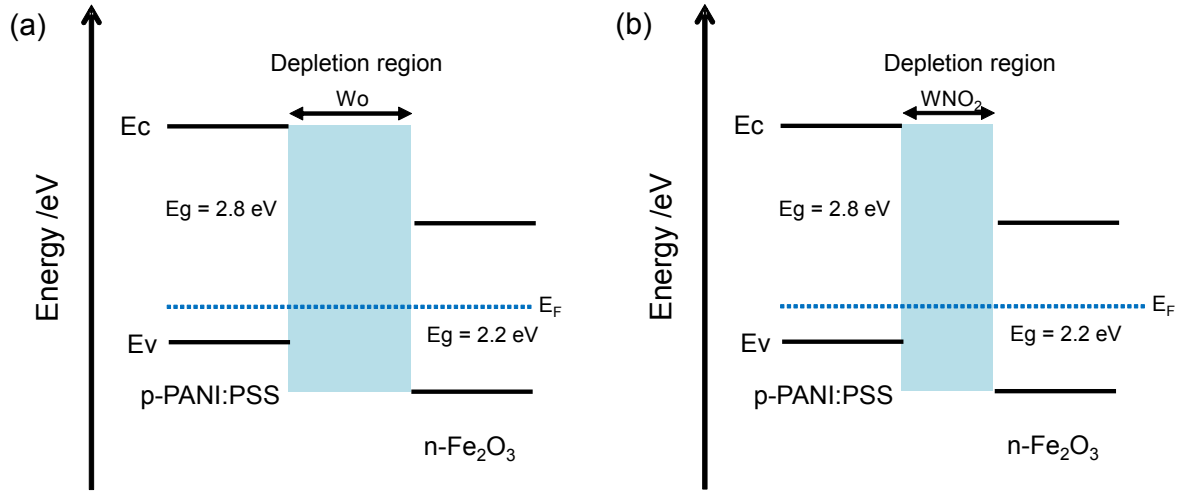

Figure S7. Energy band diagram for M_Fe/PANI:PSS paste (a) before and (b) after exposure to NO_2 molecules.

8. Response change with different temperature of the sensor electrode

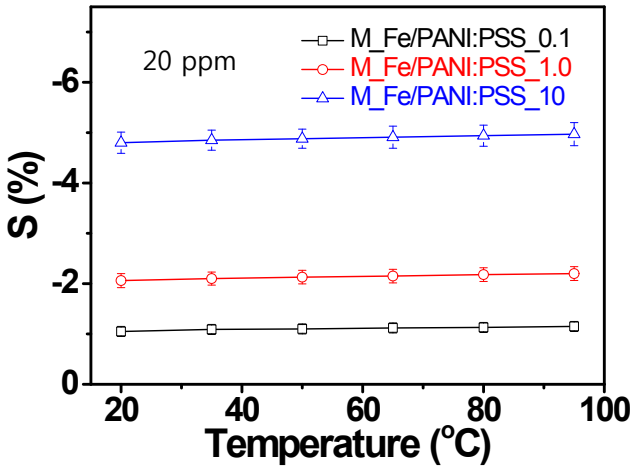

Figure S8. Calibration resistance curves of the different organic conductive nanocomposites as a function of different working temperature at 20 ppm of NO_2. (black: M_Fe/PANI:PSS_0.1; red: M_Fe/PANI:PSS_1.0; blue: M_Fe/PANI:PSS_10)

9. Response and recovery time of the sensor electrode under various temperatures

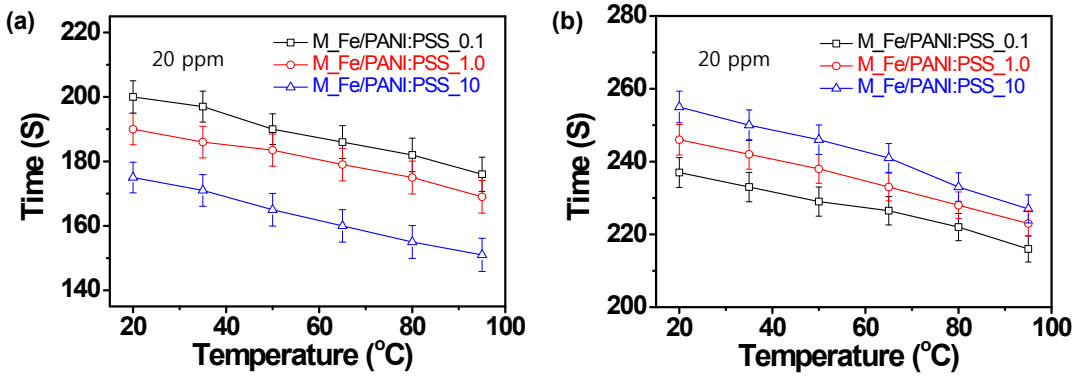

Figure S9. (a) Response and (b) recovery time of the different organic conductive nanocomposites as a function of different working temperature at 20 ppm of NO_2. (black: M_Fe/PANI:PSS_0.1; red: M_Fe/PANI:PSS_1.0; blue: M_Fe/PANI:PSS_10)

10. Response changes of the sensor electrodes with changing relative humidity

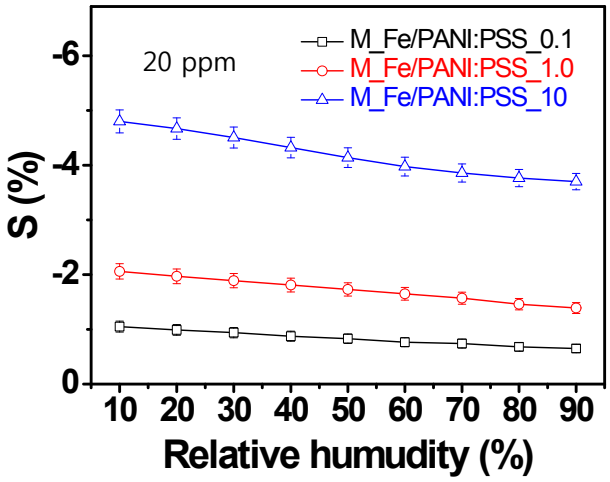

Figure S10. Calibration resistance curves of the different organic conductive nanocomposites as a function of different relative humidity at 20 ppm of NO_2. (black: M_Fe/PANI:PSS_0.1; red: M_Fe/PANI:PSS_1.0; blue: M_Fe/PANI:PSS_10)

11. Selectivity of the sensor electrode

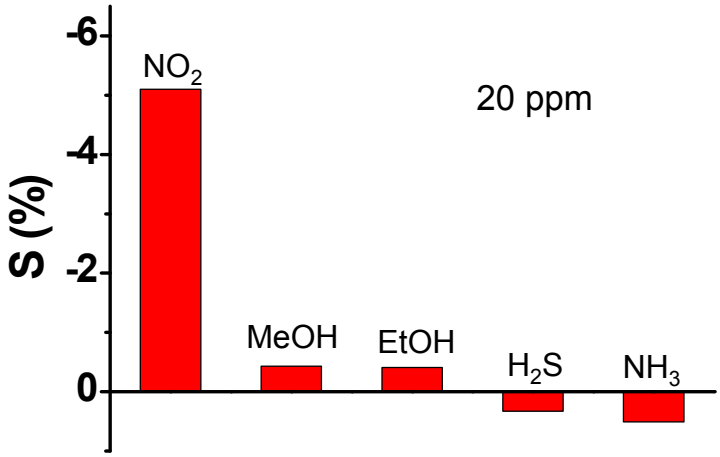

Figure S11. Response (S) changes of M_Fe/PANI:PSS-based sensor electrode to different analytes at room temperature (concentration of the chemicals is maintained at 20 ppm).

12. Schematic diagram of the wireless sensing system

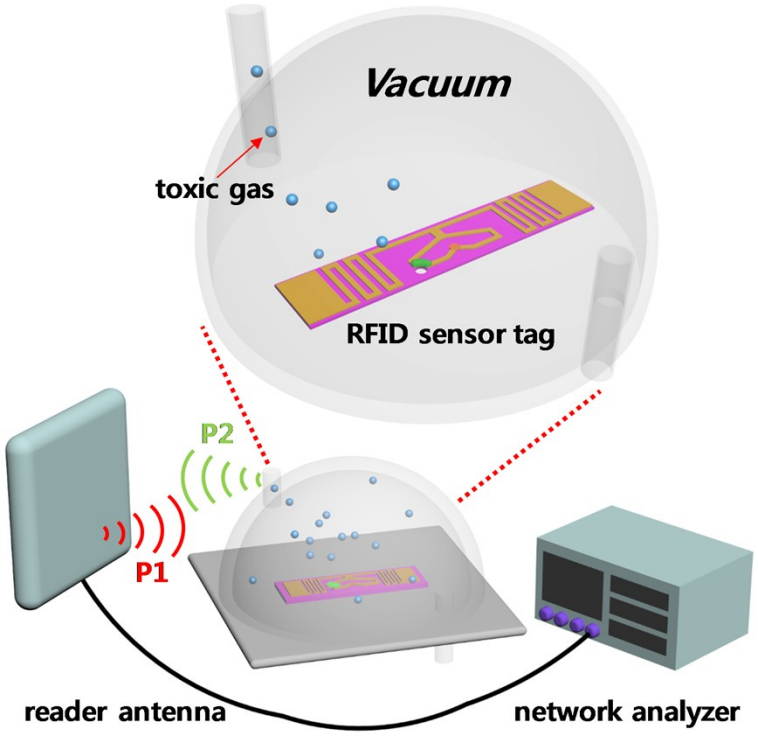

Figure S12. Schematic diagram of the RFID based-wireless sensor system consisting of reader antenna-connected network analyzer and a sensor tag.

13. Bending stability of the sensor tag

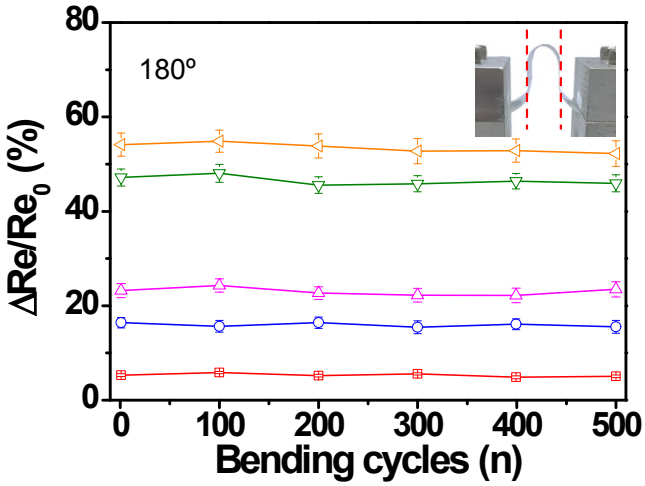

Figure S13. The normalized reflectance curves under repeated bending (180º) cycles at 10 cm distance apart with different NO_2 gas concentrations (red: 0.5 ppm; blue: 1 ppm; pink: 5 ppm; green 25 ppm; yellow: 50 ppm).